Egypt. J. Chem. **Vol. 67**, No. 8. pp. 387 - 407 (2024)

Egyptian Journal of Chemistry

http://ejchem.journals.ekb.eg/

The formation of Tetraethylene Pentaamine/Bentonite Composite with High Adsorption Effectiveness for Nickel Recovery from Leach Liquor

Haeam A. Abdelmonem[a], Elsayed A. Haggag[b], Hani E. Sharafeldin[c], Khaled A. Abd El-Rahem[d], Bahig M. Atia[b], Maram M. Mohammed[b], Mohamed S. Atrees[b], Mahamed F. Cheira[b], Adel E.-S. Goda[e]*

[a] *Chemistry Dept., Faculty of Women for Art, Science, and Education, Ain Shams University, Heliopolis, Cairo 11757, Egypt*

[b] *Nuclear Materials Authority, P.O. Box 530, Maadi, Cairo, Egypt.*

[c] *Al-Azhar University, Faculty of Engineering, Mining and Pet. Dept., Nasr City, 11371, Cairo, Egypt.*

[d] *Chemistry Department, Faculty of Science, Al-Azhar University, 71524 Assiut, Egypt.*

[e] *Tanta Higher Institute of Engineering and Technology, Tanta 31739, Egypt*

Abstract

For the recovery of nickel from Egyptian sheared serpentinized ultramafic rock leaching solution from Um Seleimat ophiolites in the south-eastern desert, a composite tetraethylene pentaamine/treated bentonite (TEPA/TB) was prepared using a wet technique. Devices including SEM, XRD, FTIR, EDS, and BET were manipulated to discover more about the TEPA/TB adsorbent after it was made. Nickel ions were adsorbed for nickel chloride solution by TEPA/TB composite. The optimal Ni ions sorption parameters were 150 mg/L Ni ions by reacting 50 mg TEPA/TB with Ni ions at pH 5 for 60 minutes at 25 °C. The TEPA/TB composite was found to have excellent sorption characteristics for Ni ions in its solution, as evaluated by the nickel recovery behaviors. The highest capacity of Ni ions taken up was 132.5 mg/g. Pseudo-second-order and Langmuir's isotherm fit the sorption mechanism quite well. Ni ions sorption onto the TEPA/TB composite was found to be an exothermic, random, and spontaneous process in the thermodynamic analyses. Using 0.7 M H_2SO_4 for 40 minutes, Ni ions were also desorbed from Ni/TEPA/TB. In addition, after eight cycles of Ni ions adsorption-desorption, the TEPA/TB sorbent was regenerated. TEPA/TB sorbent was used to recover nickel ions for serpentine-bearing rock after dissolution to gain Ni ions leachate using 4 M HCl, a stirring speed of 275 rpm, and a 1/8 S/L ratio for 4 hours of contact time at 25 °C. Finally, the Ni ions' adsorption-desorption on TEPA/TB was applied to gain a $NiSO_4$ solution, which was used to precipitate nickel as $Ni(OH)_2$. The precipitate was calcined to NiO, which has a 75.83% purity level of Ni ions.

Keywords: *Leaching, Nickel, Adsorption, Recovery, Tetraethylene pentaamine, Bentonite.*

1. Introduction

Nickel, along with iron and copper, is a particularly ubiquitous metal. The primary minerals that contain nickel can be categorized into sulfides and oxides. Nickel production relied heavily on sulfide ores in the bygone days. With the depletion of high-grade nickel sulfide ores, the nickel production industry is shifting its focus to nickel oxide or laterite ores, which boast more attractiveness [1,2]. Nickel is sixth in abundance on the earth after iron, oxygen, silicon, and magnesium. About 3% of the earth is nickel. Most nickel occurs in mafic or basic rocks. Dark, dense mafic rocks are iron and magnesium-rich. Acid or silicic rocks, high in silicon and light-colored, have little nickel content. Most rocks with

*Corresponding author e-mail: adelgoda1969@ gmail.com.
Received date 26 December 2023; revised date 29 January 2024; accepted date 31 January 2024
DOI: 10.21608/EJCHEM.2024.258292.9080

more iron and magnesium and less silicon and aluminum have more nickel. Nickel-bearing minerals' principals are sulfide and oxide [3,4]. Making coins is the most important usage of this element. It is a component of wires. Because it can withstand high temperatures without corroding, it finds usage in gas turbines and rocket engines. Armor plating, nails, and pipes are all made from alloys that include it. Nickel and copper alloy monel is resistant to corrosion in saltwater because it is a complex compound. This is why you'll find it in desalination plants and boat propeller shafts [5-7].

The laterite (oxide) mineral group accounts for almost 70% of the world's ferrous metal reserves. Thirty percent of the nickel reserves are in sulfide minerals. Most of the world's nickel comes from pentlandite, the most prevalent nickel sulfide mineral. Additionally, millerite, heazlewoodite, and polydymite are significant nickel sulfide minerals. Nickel oxide minerals that are frequently mined include garnierite and nickeliferous limonite. Oxide minerals, in contrast to sulfide minerals, have nickel concentrations that are low and highly changeable. Because of the way they originate, oxide ores are often referred to as lateritic ores [8,9].

Technologies have been created to enable the commercially viable processing of nickel ores. Pressure and atmospheric acid leaching with sulfuric acid as a leaching agent are two of these methods for dissolving nickel [10,11]. Additionally, Ni ions were extracted from saprolitic laterite ores using hydrochloric acid [12]. Additionally, nickel was leached from limonite ore using a solution of 2 M citric acid and 0.5 M sulfuric acid and from saprolite ore using a solution of 0.5 M citric acid and 2 M sulfuric acid [13]. For each metabolic acid (citric, oxalic, and acetic), the dissolution kinetics of nickel laterite ore in water-based acid solutions were studied separately in a batch reactor [14]. Variations in solution concentration and operating time were used to carry out the laterite nickel leaching procedure. Solution concentrations of sulfuric acid and phosphoric acid ranged from 5 M to 6 M, and operation times were changed from 4 to 6 hours [15]. Several methods are used to remove nickel ions from the leaching liquid, including precipitation [16,17], ion exchange [18], solvent extraction [19,20], and adsorption [21-23]. Since adsorption is so effective, easy to implement, and inexpensive, it has attracted a lot of attention from researchers working on nickel ion removal. Some examples of materials that have been successfully used as adsorbents include activated carbon [24], resins [25], zeolite [26], silica microparticles [27], kaolin [28], ethylenediamine/silica gel [29], etc.

The utilization of clays as a sorbent has several benefits compared to commercially available alternatives. These include their inexpensive cost, plentiful obtainability in nature, high surface area, tremendous sorption capabilities, non-toxicity, and high prospective for ion exchange [30]. Cations in clays can be exchanged for anions that are left on the surface. Because of these reasons, researchers all over the globe have been looking at clays, both natural and artificial, as potential sorbents for the elimination of heavy metals from waste solutions [31]. The binary solution of Ni ions and Mn ions was isolated using the unaltered kaolinite clay [32].

These days, there are a plethora of studies that detail how clays, in their different modified forms. Ni ions were adsorbed from a water solution at pH 6 using sodium pyrophosphate/bentonite, with an adsorption rate of 30.3 mg/g [33]. $CuFe_2O_4$/bentonite composite was effectively made to adsorb 99.1% Ni ions from electroplating wastewater through the use of a chemical co-precipitation technique at pH 5 [34].

Batch adsorption-equilibrium studies were conducted at pH 5.5 to examine the efficacy of magnetically modified bentonite in removing nickel from water-based solutions [35]. Montmorillonite and Ca-montmorillonite adsorb 73 mg/g of nickel ions from acid solutions at a pH 7 [36]. Nevertheless, a solution of epichlorohydrin, chitosan, and clay was employed to remove nickel from water at a pH of 6, resulting in adsorption of 32.36 mg/g [37]. There was an absorption of 6.32 mg/g of nickel cations in the waste waters of galvanic businesses using Ca-bentonite and Na-bentonite [38]. Chitosan immobilized on bentonite was used to examine the sorption of Ni ions from solutions at a pH of 5.5 [39]. Additionally, in an aqueous media, Ni ions adsorbed on ZrO-kaolinite surfaces at an uptake of 8.8 mg/g and on ZrO-montmorillonite surfaces at an uptake of 22 mg/g, respectively [40].

This study describes the development and evaluation of a sorbent made of treated bentonite and tetraethylene pentaamine (TEPA/TB) for the purpose of adsorbing and recovering Ni ions from leach

liquid. Sorption isotherms, uptake kinetics, pH, and TEPA/TB dose are all used to evaluate TEPA/TB's sorption properties. The important thermodynamic and kinetic properties besides isotherms are also evaluated. We examine the sorption characteristics. Nickel desorption and recycling are other areas of evaluation for TEPA/TB sorbent. The leaching parameters, which are leaching temperature, solid/liquid ratio, agitation time, stirring rate, and hydrochloric acid concentration, are investigated. The optimal parameters are applied for recovering nickel ions from the leach solution.

2. Materials and Methods

2.1. Materials

All of the substances applied in the experimentation were analytically pure. Sodium hydroxide (NaOH, 98.2%), ethyl alcohol (CH_3CH_2OH, 99.5%), sodium chloride (NaCl, 99%), hydrochloric acid (HCl, 36.5%), tetraethylene pentaamine ($C_8H_{23}N_5$, 99%), and N, N-dimethylformamide ($HCON(CH_3)_2$, 99.5%) were all purchased from Sigma-Aldrich. A Ni ions standard solution with a concentration of 1000 mg/L was prepared by accurately weighing and dissolving $NiCl_2$ in 10 mL of HCl (36.5% concentration) in 1 L of purified water.

2.2. Analyses and Descriptions

All samples were measured for nickel ion content using atomic absorption spectrophotometers (AAS, model: Analyst 700 paired with MHS-15 from Perkin Elmer Instruments, USA). The analytical technique known as X-ray fluorescence (XRF) exploits the interaction of X-rays with bentonite, TB, and serpentine-bearing rock to detect their compositions. Scanning electron microscopy (FEI QUANTA FEG 650) was used to examine the surface and structural properties of bentonite, TB, and TEPA/TB. Simultaneous analysis of the element composition of bentonite, TB, and TEPA/TB was carried out using scanning electron microscopy (SEM) and energy-dispersive X-ray spectroscopy (EDX, Inc. Genesis XM). The surface functional groups were determined using Fourier transform infrared spectroscopy (FTIR) on a Nicolet 6700 between 400 and 4000 cm^{-1}. Fifty scans were made at a resolution of 2 cm^{-1}. Using the Brunauer-Emmett-Teller (BET) method and N_2 adsorption isotherm measurements on a Quadrasorb Si-MP surface area analyzer, the specific surface area and porosity properties of bentonite, TB, and TEPA/TB were determined. A pleasant 77 K was reached in the room where these readings were taken. To evaluate the surface chemical composition of the materials under study, X-ray diffraction (XRD) was performed using a D8 advance Bruker spectrometer and a PHI 5000 versa probe spectrometer. At 150 °C for 3 h, the samples were first out-gassed under a vacuum of 10^{-4} Torr. A zeta sizer examination was carried out to ascertain the pH of the isoelectric point (pH_{IEP}). The instrument used for this analysis was a nano-series zeta (Nano-ZS Malvern Instruments Ltd., Malvern, UK).

2.3. Sample Formulation

A technically typical sample of the raw ultramafic rocks carrying serpentine minerals was formed by collecting a sample of Um Seleimat sheared serpentinized rock [41]. Ultramafic rocks are widespread in the central and southern eastern desert of Egypt, covering about 5.3% of the basement complex of Egypt [42]. They occur as serpentinized masses of all dimensions ranging from mountainous ranges down to small lenses measuring at the scale of a few centimeters. The serpentinites are variably transformed into talc-carbonate rocks. Such transformation is more pronounced in the small lenticular serpentinite masses and along shear planes [43-45].

Raw serpentine-bearing ultramafic rocks, also known as sheared serpentinized on ultramafic rocks, were mined in the southeastern desert of Egypt, specifically in the Um Seleimat area. The serpentine-bearing ultramafic rocks are located in Um Sleimat area, which is a tributary from Wadi Nugrus. This area is accessible by cars. It is accessible about 5 km from the entrance of Wadi Nugrus at its junction with Wadi El-Gemal. It was detected mineralogically and determined analytically. Crushing, grinding, screening, and correct quartering were used to prepare the sample for this study. In order to remove contaminants from the leach liquor and recover the nickel ions, the solutions that were generated following the leaching trials underwent extraction methods.

2.4. Characteristics and Treatment of Bentonite

B Bentonites are colored greenish, yellowish green, bluish green, reddish grey, and grey. When they dry, they take on a lighter hue. The International Co. supplied the Egyptian bentonite utilized in this inquiry for mining and investments in Egypt, and it came from the El Fayoum region. Pretreatment and additional clay modification are necessary to stop heavy metal leaching, according to preliminary adsorption results. The pretreatment procedure was completed to obtain a sodium version of bentonite.

Two phases of the natural bentonite curring were carried out. Raw clay, weighing 150 g, was first treated with a 1.5 L solution of 0.8 M hydrochloric acid at 25 °C for 6 hours. The silt was filtered and rinsed with water until the clay was free of chloride ions. It was then dried at 80 °C after reaching a pH range of 6 to 6.5, as determined by a 0.1 M silver nitrate solution. After that, the 50 g of bentonite clay was subjected to a second round of treatments by being refluxed for 36 hours at 80 °C in a flask with 1.5 L of a 1.5 M NaCl solution. Using 0.1 M silver nitrate, the resulting suspension was centrifuge-separated and rinsed multiple times with distilled water until no chloride was discovered. For the last step, the chloride-free samples were carefully ground and oven-dried at 80 °C. They will be stored for future use. Bentonite, both natural and activated, and its main chemical components are listed in Table 1.

Additionally, SEM-EDX and X-ray diffraction (XRD) investigations were used to characterize bentonite. Bentonite is an aluminosilicate substance due to its high SiO_2 and Al_2O_3 content, while high-silica montmorillonite is rich in potassium, sodium, and magnesium [46]. Octahedral aluminum sheets and silica tetrahedral sheets are the structural building elements of bentonite clay. Two tetrahedral silica sheets and one aluminum octahedron make up a single-unit cell [47].

Table 1.
Natural and treated bentonite chemical scrutiny using XRF

Components	Natural B (%)	TB (%)
SiO_2	56.17	59.42
Fe_2O_3	5.03	2.42
Al_2O_3	17.16	15.57
CaO	4.12	2.34
TiO_2	0.12	0.12
K_2O	1.76	0.67
MgO	3.14	1.32
Na_2O	4.11	8.34
P_2O_5	0.14	0.11
MnO	0.15	0.14
LOI[a]	7.44	9.13

LOI: At 1000 °C, there is a loss of ignition.

2.5. TEPA/TB Preparation

The wet technique was used to prepare the TEPA/TB composite material [48]. The first step was to combine 20 g of TB powder with 200 mL of deionized water in a conical flask. Mechanical agitation at 300 rpm and ultrasonic dispersion at 200 W for 15 minutes were employed to achieve TB dispersion. The second step was to form a TEPA/TB adsorbent by dissolving 6 g of TEPA powder in a suspension and then mechanically agitating the mixture for 120 minutes. The filter cake was obtained by subjecting the ternary suspension to 20 minutes of sitting time and then using vacuum suction to filter it. It was then washed three times with deionized water. A vacuum drying process at 62 °C for 24 hours was the final step in effectively fabricating TEPA/TB powder.

2.6. Leaching Development

In order to dissolve the majority of nickel components with minimal solubility of other undesirable compounds, acidic leaching procedures were studied and kept up to date. In a 300 mL Teflon beaker, the leaching processes were carried out under varying conditions, including different kinds of acids 2M (H_2SO_4, H_3PO_4, HCl, and HNO_3), different concentrations of HCl (0.5-6 M), solid-to-liquid ratios ranging from 1/3 to 1/10, leaching times ranging from 0.5 to 6 hours, stirring degrees from 125 to 375 rpm, and temperatures from 25 to 80 °C. The samples were transported at various parameters and tested to see how the leaching processes improved. After the leaching process was completed, the deposit was extracted and washed with distilled

water. We performed a quantitative analysis on the leaching liquid that we received. These are the formulae that were used to determine the nickel leaching efficiencies.

$$leaching\ efficency, \% = \frac{Ni\ dissolved\ in\ solution\ (mg)}{Ni\ total\ amount\ in\ solid\ (mg)} \times 100 \quad (1)$$

2.7. Sorption Evaluations

Experiments in which Ni ions were removed from a solution in batches allowed us to examine the adsorption behavior of the produced TEPA/treated bentonite. To determine the optimal sorption conditions, several tests were run in an isothermal shaker (270 rpm) using 50 mL of the aqueous solution with an initial nickel concentration of 150 mg/L and varying doses of TEPA/TB (10-100 mg), pH (1-9), sorption temperature (25-55 °C), and sorption time (5-120 min). With the use of a Hanna pH meter and some diluted 0.2 M of HCl and NaOH solutions, the pH of the test solutions was determined. The solid TEPA/TB sorbent was filtered out at equilibrium using Whatman filter membrane paper after agitation. Using an atomic absorption spectrometer, the concentration of nickel ions in both the filtrates and the starting solution was calculated. The subsequent equation was used to get the equilibrium percentage of removal:

$$Removal\ (\%) = \frac{C_0 - C_{eq}}{C_0} \times 100 \quad (2)$$

where C_0 and C_{eq} are the initial and equilibrium nickel concentrations in the liquid phase (mg/L). The equation was used to determine q_e (mg/g) as the quantity of nickel adsorbed by one gram of TEPA/TB sorbent under equilibrium circumstances.

$$q_e = \frac{(C_0 - C_{eq})v}{m} \quad (3)$$

m = amount of TEPA/TB sorbent in grams, where v = volume of leaching solution in liters.

3. Results and Discussion

3.1. Adsorbent Characterization

3.1.1. XRD Analysis

Mineralogical testing revealed that natural B, TB, and TEPA/TB are basically montmorillonite [49]. Natural B is mostly montmorillonite, with trace amounts of quartz, kaolinite, and calcite, according to the data shown in Figure 1a. The various peaks of montmorillonite can be seen in the XRD spectrum of the TB data in Figure 1b at 2θ = 7.12° (d= 9.89 Å), 20.02° (d= 5.45 Å), and 2Ÿ= 26.98° (d= 4.23 Å). Figure 1c shows results that are consistent with the TEPA/TB XRD pattern. With a decrease in the d-value from 9.89 Å for the TB to 6.45 Å for the TEPA/TB, the displacement and smallest angle 2θ go from 7.12° to 6.75°, respectively. This allows the TEPA to be inserted into the interlayer space while simultaneously expanding the montmorillonite layers. The XRD data shows that between 4° and 80°, there is a good match between NB and various bentonite forms. This suggests that the bentonite structure was unaffected by the treatment and conversion operations.

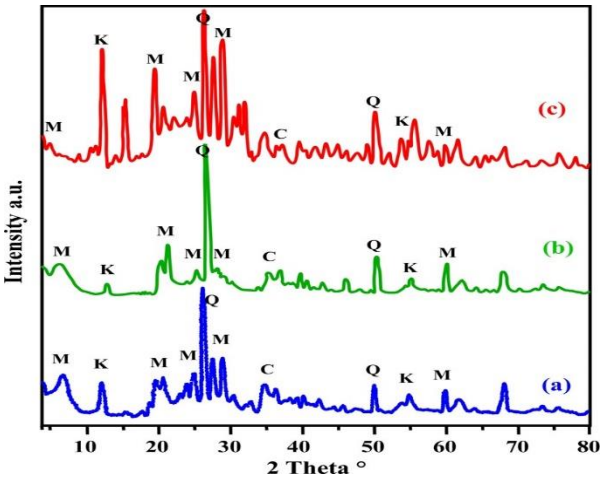

Figure 1. The XRD scale of **(a)** natural B**, (b)** TB, and **(c)** TEPA/TB

3.1.2. Surface Analysis

The surface area and structures of natural B, TB, TEPA/TB, and Ni/TEPA/TB were evaluated using the BET equation, which was derived using N_2 adsorption-desorption isotherms at 77 K. The surface area, pore volume, and pore size of TB were 1.99 m^2/g, 0.189 cm^3/g, and 116.6 nm, respectively, as shown in Table 2. The organic moieties were better dressed, and the TB trapped the Ni ions due to their large surface area and small pore size. From 2.47 to 2.65 m^2/g, the surface areas were raised by the TEPA/TB and the Ni/TEPA/TB. Aside from that, the pore size shrank from 112.8 to 110.8 nm, and the pore volume fell from 0.233 to 0.218 cm^3/g. According to the findings, the tetraethylene pentamine was effectively strengthened within the tuber without damaging the pore spaces. The making of

Ni/TEPA/TB led to a reduction in the pore volume and size of TEPA/TB to 0.218 cm^3/g and 110.8 nm, respectively, after nickel sorption.

Table 2.
Surface area, pore size, and volume of natural B, (b) TB, TEPA/TB, and Na/TEPA/TB

	S_{BET}, m^2/g	Pore volume, cm^3/g	Pore size, nm
Natural B	1.21	0.177	125.3
TB	1.99	0.189	116.6
TEPA/TB	2.47	0.233	112.8
Ni/TEPA/TB	2.65	0.218	110.8

3.1.3. SEM Analysis

The scanning electron micrograph of natural bentonite, TB, TEPA/TB, and Ni/TEPA/TB is given in Figure 2. Figure 2a shows the SEM morphology of bentonite's surface, which consists of a heterogeneous, smooth surface with several pores inside and condensed particles with tightly damaged, irregular, and distorted surfaces. Figure 2b shows the SEM depiction of TB, which reveals irregularly assembled particles, apparent porosity, and a rough surface. Pore formation and small size form on the surface of TEPA/TB, with disturbed and agglomerated particles responsible for the sorption of Ni ions (Figure 2c). The Ni ions sorption on the TEPA/TB surface may be seen in the SEM image in Figure 2d, which exhibits noticeable microscopic porosity and a rough surface of materials with emerging spots on the surface spaces.

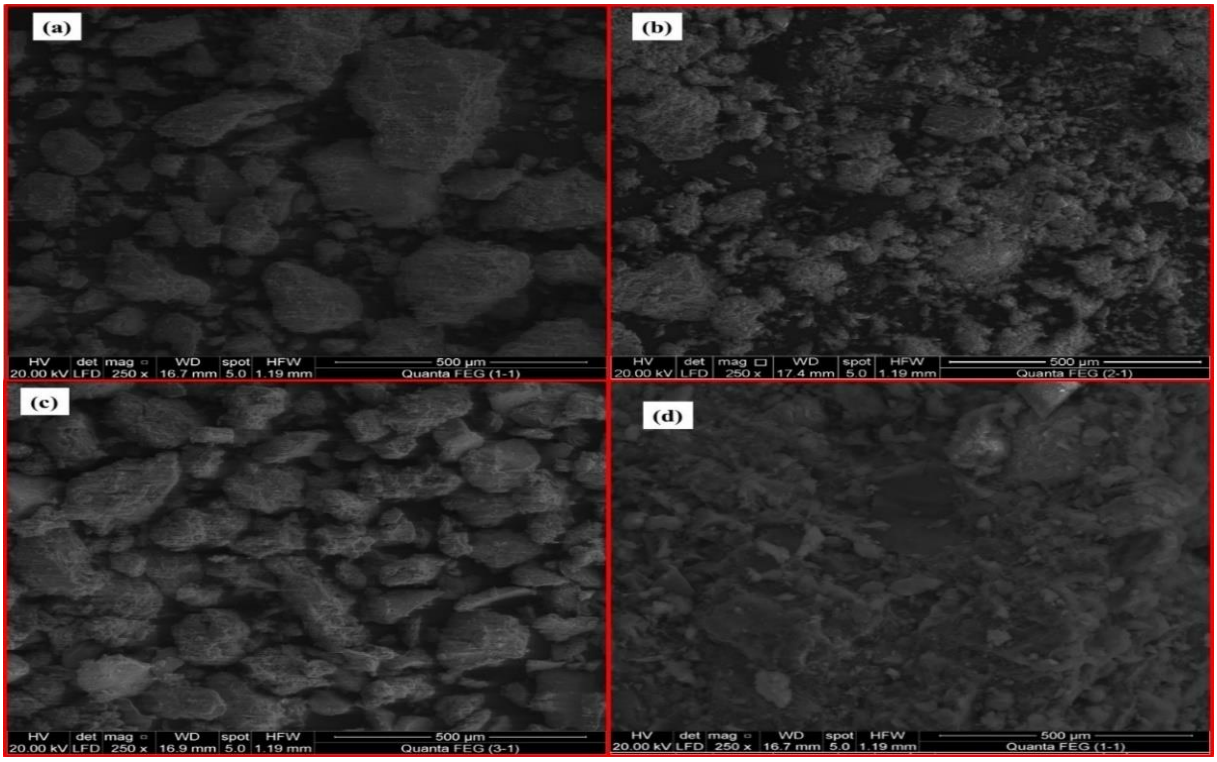

Figure 2. SEM study **(a)** natural bentonite, **(b)** TB, **(c)** PETA/TB, **(d)** Ni/PETA/TB.

3.1.4. EDX Investigation

EDX analysis discovered that virtually all metal ions are released from natural bentonite, which is treated with HCl and NaCl to obtain treated bentonite (Figure 3a, b). The EDX spectrum of TEPA/TB shows carbon and oxygen atoms at the ranges; TEPA reacts in the interlayer of TB by hydroxy groups, and H_2O is released (Figure 3c). Moreover, The TEPA/TB adsorbed Ni ions due to the presence of Ni ions peaks in Figure 3d. Hence, EDX data confirmed

that Ni ions were adsorbed and trapped onto the TEPA/TB sorbent.

3.1.5. FT-IR Analysis

The FT-IR evaluations for natural B, TB, TEPA/TB, and Ni ions loaded on TEPA/TB were carried out and assumed in Figure 4. The broad peaks of natural and TB existed at 3419 and 3418 cm^{-1} for the combining SiO-H or AlO-H and OH stretching of H_2O (Figure 4a, b). Moreover, The bands at 1643 and 1652 cm^{-1} are recognized as the OH deformation of H_2O adsorbed on the bentonite surface. The peaks at 1039 and 444 cm^{-1} (natural B), besides at 1043 and 449 cm^{-1} (TB), were spotted for Si–O stretching and bending vibration, which specified tetrahedral bending manner, while the peaks at 931 and 543 cm^{-1} (natural B), besides at 927 and 547 cm^{-1} (TB) for Al–O stretching and bending peaks are matching to octahedral manner [50].

The presence of amine bands of tetraethylene pentamine/treated bentonite qualitatively supports the realization of the functionalization of TB. The OH stretched at 3370 cm^{-1} of TB, while the bands were at 3315 and 3211 cm^{-1} for amino groups in TEPA/TB (Figure 4c).

In the Ni ions sorption on TEPA/TB, these peaks were combined and moved to 3395 cm^{-1} (Figure 4d). The symmetric and asymmetric stretching modes of the C-H bonds in the $-CH_2-$ and $-CH_2-NH_2$ groups of TEPA/TB are thought to be responsible for the new bands seen at around 2957 and 2872 cm^{-1}, respectively, [51]. The symmetric and asymmetric bending of primary amines is responsible for the bands observed at 1485 and 1551 cm^{-1}, respectively. The vibrational bending of the molecules devoid of water changed to 1668 cm^{-1} [52]. Ni ions adsorption significantly increased the strength of the C-N single bond, leading to a small rise in the C-N band stretching frequency from 1263 to 1107 cm^{-1} [53]. Additionally, as a result of the redshift-related shifting, certain peaks emerged at distinct wavenumbers. It appears that the Ni ions were adsorbed into the TEPA/TB surface.

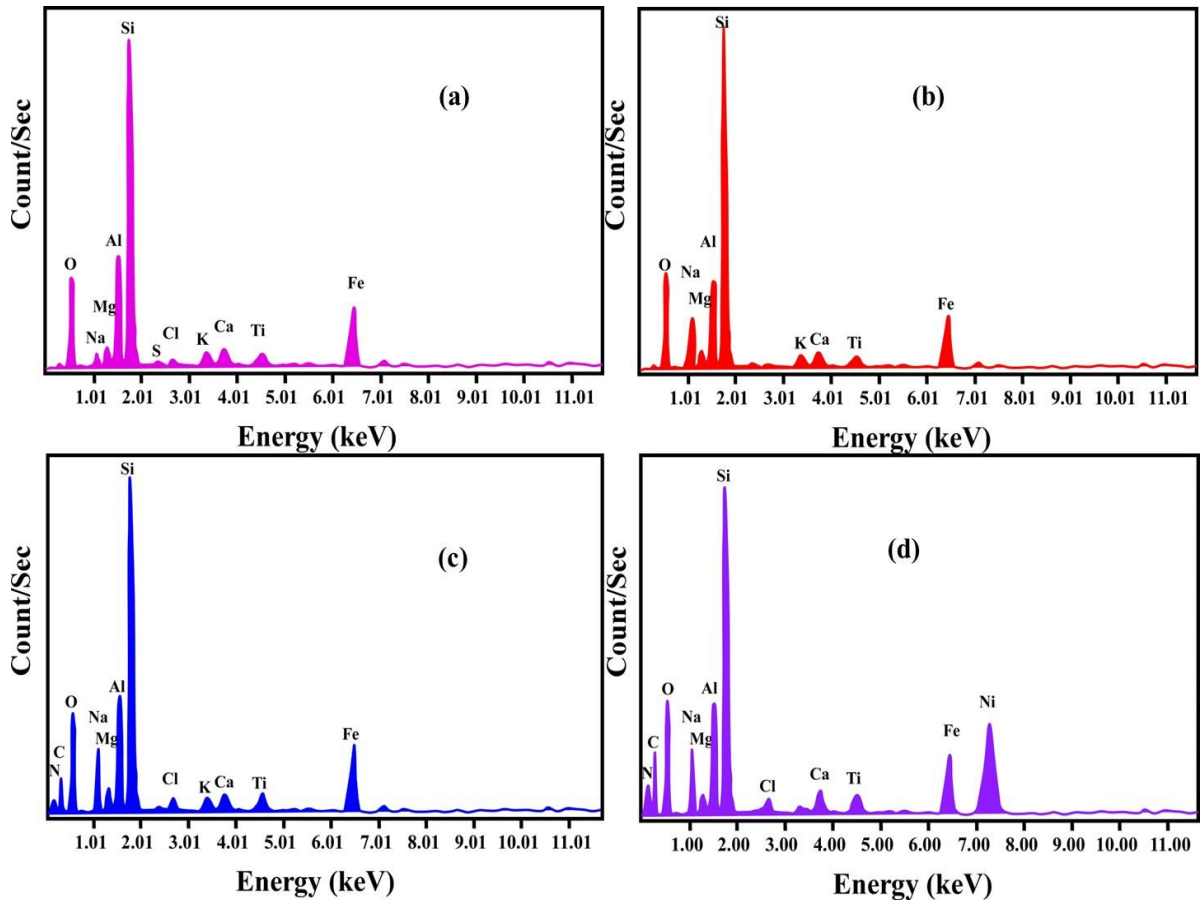

Figure 3. EDX analysis **(a)** natural B, **(b)** TB, **(c)** TEPA/TB, **(d)** Ni/TEPA/TB

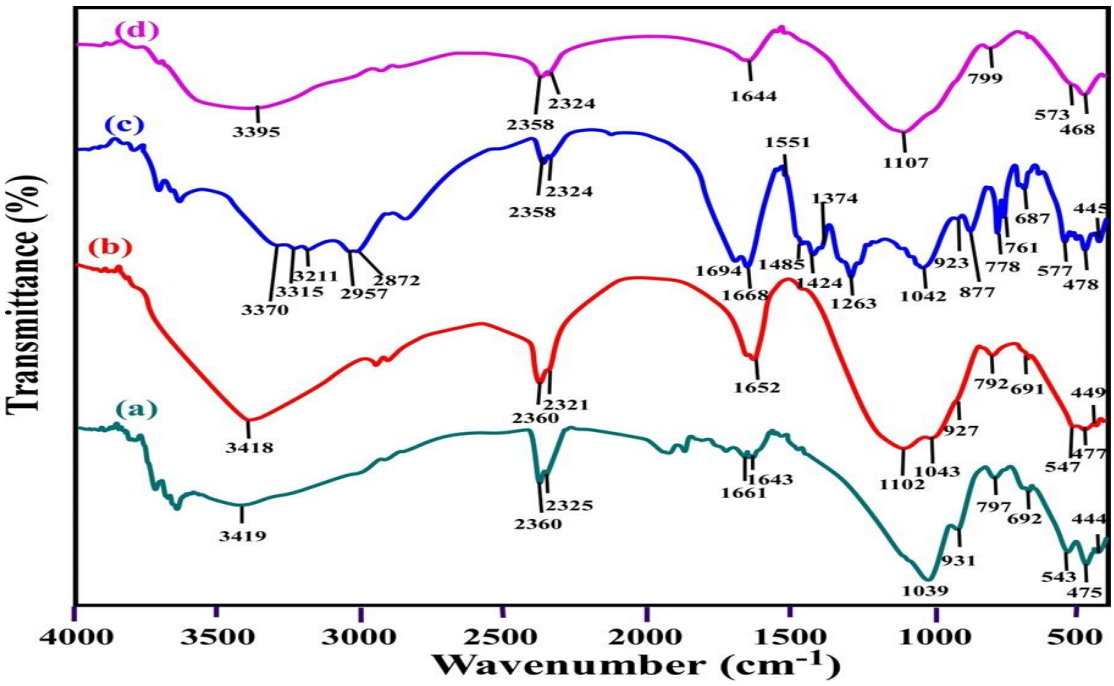

Figure 4. The FT-IR evaluations of **(a)** natural B, **(b)** TB, **(c)** TEPA/TB, and **(d)** Ni/TEPA/TB

3.2. Ni ions Sorption by TEPA/TB

The current investigation used TEPA/TB as an adsorbent to extract Ni ions from a Ni ions solution with a 150 mg/L concentration. The Ni ions solution has been optimized by doing many sets of equilibrium tests on the following parameters: pH, contact time, TEPA/TB dosage, initial concentration of Ni ions, and temperature.

3.2.1. pH Impact

When it comes to the adsorption of Ni ions on the TEPA/TB, solution pH is a major factor (Figure 5a). The effects of pH on the capacity of the TEPA/TB adsorbent to remove Ni ions are studied throughout a pH range of 1 to 9. All other experimental parameters remain constant, including a 50 mL volume of 150 mg/L Ni ions in contact with 50 mg of TEPA/TB for 60 minutes at room temperature. Adsorption of Ni ions increases with increasing pH from 1.0 to 5.0 and subsequently decreases with increasing pH up to 9.0. The main explanations for this result could be due to a variety of events, such as the precipitation of Ni ions (e.g., hydroxide) or a change in the surface charge of the TEPA/TB at high pH. There are fewer Ni ions in the solution and less chance of it being adsorbed by the adsorbent under study because of this precipitation. In addition, the presence of Ni ions causes repulsive electrostatic forces to be generated between the TEPA/TB surface and the ions when the surface charge is changed to negative [54]. Together, these occurrences ultimately lower the TEPA/TB's Ni ions removal efficiency. It was established as the optimal value since the maximum efficiency of Ni ions removal was achieved with an initial pH of 5.

Figure 5b indicates the governing species of Ni ions are demonstrated as Ni ions at pH<10, $Ni(OH)^+$ at pH 8–10.5, $Ni(OH)_2^0$ at pH 8.3-12, and $Ni(OH)_3^-$ at pH>9.5. This identifies that = Ni ions sorption is controlled by the ion exchange development among Ni ions and H_3O^+ on the TEPA/TB surface at minimal pH. Definitely, there is competition for sorption sites amongst Ni ions and H_3O^+ at minimal pH rates, which additionally influences Ni ions' sorption onto the TEPA/TB surface. Hence, Ni ions ionic species (Ni ions and $Ni(OH)^+$) are pretty sorbed at the negatively charged TEPA/TB surface at pH 5. The majority of Ni ions ($Ni(OH)_2^0$ and $Ni(OH)_3^-$) face severe electrostatic repulsion against the

negatively charged surface of TEPA/TB. The negatively charged surface of TEPA/TB strongly electrostatically repels most nickel compounds, including $Ni(OH)_2^0$ and $Ni(OH)_3^-$.

The Zeta potential of TEPA/TB can also shed light on the pH effect, as shown in Figure 5c. Results show that TEPA/TB has a pH_{IEP} value of 4.85. At a pH<4.85 (the isoelectric point, pH_{IEP}), the surface of TEPA/TB became positively charged due to protonation. This protonation effect is more pronounced at lower pH levels due to the increased concentration of H_3O^+ ions in the solution, which is detrimental to the sorption of Ni ions. Ni ions are able to adsorb onto the surface charge groups of TEPA/TB when the pH is higher than 4.85 because the structure of TEPA/TB gains more negative charges. The strongly negatively charged TEPA/TB could attract the positively charged Ni ions. When the pH of the solution is more than 4.85, negative charges start to form on the surface of the TEPA/TB, and the zeta potential is at its highest absolute value at pH 5. There is a high Ni ions sorption by TEPA/TB at this pH.

3.2.2. TEPA/TB Dose Impact

With a pH of 5, 50 mL of a solution inspecting 150 mg/L of Ni ions, and 60 minutes of contact time at room temperature, this study found that adsorbent doses ranging from 10-100 mg were effective in removing Ni ions using TEPA/TB adsorbent. Figure 5d shows the acquired data, which shows that the removal efficiency has risen with improving the TEPA/TB dose. This is because, at larger doses, there are more ion exchange sets existing for ion exchange systems due to the increased surface area. Thus, from 10 to 60 mg of TEPA/TB, the removal efficiency of Ni ions rose from 17.66% to 98.5%. Up until 100 mg, the adsorption efficiency was consistent..

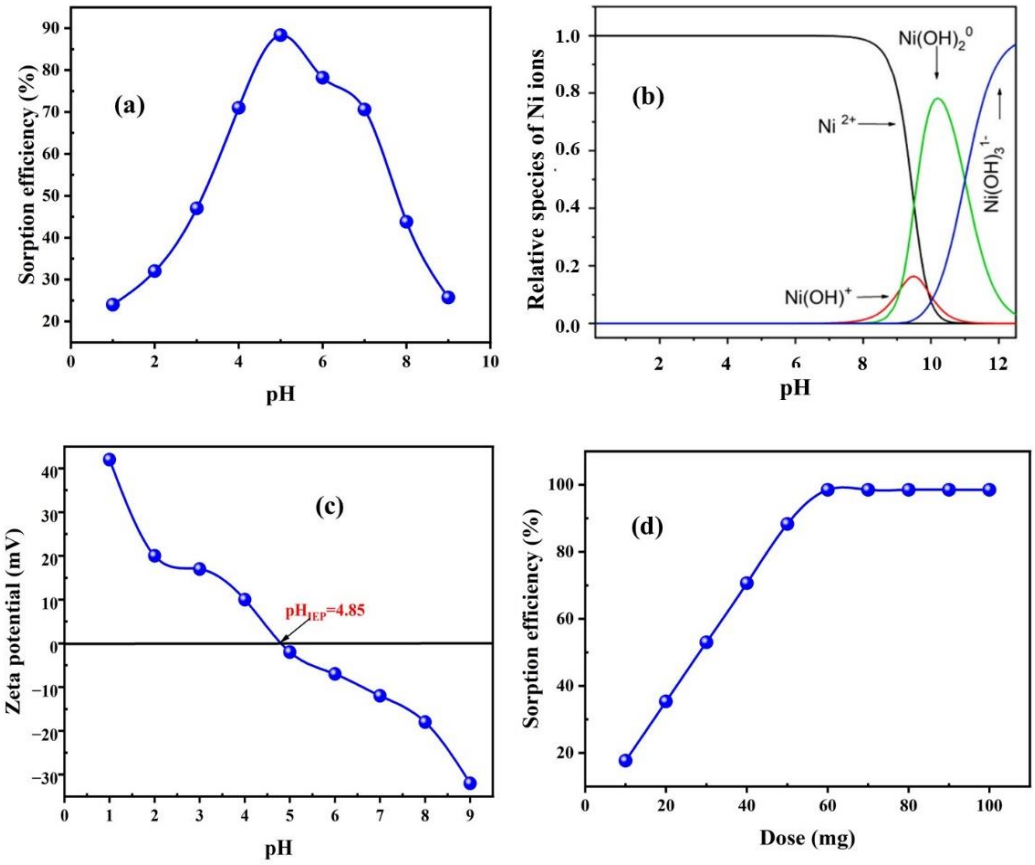

Figure 5. (a) pH impact of Ni ions sorption on TEPA/TB (150 mg/L Ni ions, 50 mg TEPA/TA, 60 min contact, 50 mL, 298 K), **(b)** distribution of Ni ions species in solution (2.55×10^{-3} M Ni ions, (150 mg/mL Ni ions)), **(c)** Zeta potential *vs.* pH for TEPA/TB, **(d)** TEPA/TB dose impact on Ni ions sorption (50 mL, 150 mg/L Ni ions, 60 min contact, pH 5)

3.2.3. Contact Time and Kinetics

While earlier experimental settings utilized 50 mg TEPA/TB dose and 50 mL, 150 mg/L Ni ions at room temperature, this study examined the impact of contact time on Ni ions removal efficiency for TEPA/TB at different contact times extending from 5-120 minutes. The removal efficiency of Ni ions on the TEPA/TB adsorbent rose from 29.24% to 88.33% as the contact duration was increased from 5 minutes until equilibrium was reached after approximately 60 minutes, as defended in Figure 6a. Ni ions' sorption is unaffected by improving the contact period to 120 minutes. Therefore, a 60-minute contact time was taken into account for further condition optimization.

The sorption kinetics of Ni ions are studied on the TEPA/TB adsorbent in order to understand and evaluate the sorption process and sorbent performance. In order to predict the adsorption kinetics of Ni ions on TEPA/TB, experimental data is used in conjunction with various kinetics models, such as pseudo-first-order (PFO) and pseudo-second-order (PSO). To find the linearizer in PFO form, use the following equation [55,56]:

$$\log(q_e - q_t) = \log q_e - \left(\frac{k_1 t}{2.303}\right) \quad (4)$$

In which q_e (mg/g) represents the uptake of Ni ions at equilibrium, q_t (min) represents the uptake at time t, and k_1 (1/min) represents the rate constant of PFO. The kinetic mechanism is supported by the relationship between log (q_e-q_t) *vs.* t. Figure 6b and Table 3 show that the adsorption mechanism's q_e and correlation coefficient R^2 do not match a PFO kinetic mechanism. This data suggests that the PFO reaction is not a good fit for Ni ions sorption onto TEPA/TB. The PSO kinetic is run and regulated in the resulting equation [57,58]:

$$\frac{t}{q_t} = \frac{1}{k_2 q_e^2} + \frac{t}{q_e} \quad (5)$$

The amount of Ni ions adsorbed at time t (min) is represented by q_t (mg/g), the amount of adsorption at equilibrium (q_e, mg/g), and the rate constant of the PSO equation is k_2 (g/mg.min). A straight line representing Ni ions on TEPA/TB with a high correlation coefficient (0.999) close to one, as seen in Figure 6c and Table 3, indicates that the PSO mechanism is applicable. Finally, the value of the equilibrium uptake amounts (q_e) should be very near to the realistic uptake amounts (q_{exp}). These findings provide strong evidence that the PSO kinetic adsorption principle was adequately followed by the Ni ions ion sorption on the TEPA/TB adsorbent.

Table 3.
Ni ions sorption kinetic parameters of TEPA/TB

Practical uptake	PFO			PSO		
q_{ex}	q_e	k_1	R^2	q_e	k_2	R^2
132.5	206.20	0.075	0.883	136.98	4.95×10^{-4}	0.991

3.2.4. Initial Ni Ions Concentration and Isotherms

The most important sorption system characteristics that can affect the sorption behavior of Ni ions on the TEPA/TB adsorbent are the effects of the initial concentration of specific metal ions. In order to illustrate how varying the starting concentration of Ni ions impacts the removal efficiency of TEPA/TB adsorbent, many batch tests are conducted. During the trials, 50 mL containing Ni ions ranging from 25 to 800 mg/L are mixed with 50 mg of TEPA/TB adsorbent and left to shake at room temperature for 60 minutes.

In Figure 6d, we can see that the most excellent removal efficiency was achieved at an initial concentration of 150 mg/L, that the concentrations of Ni ions rose, and that the amount of Ni ions sorption (q_e in mg/g) also increased. The TEPA/TB adsorbent has a Ni ions removal capacity of 132.50 mg/g, based on an 88.33% removal efficiency at 150 mg/L. Once that point has passed, the effective adsorbent has attained its saturation capacity, as the number of Ni ions removed has stayed constant. The TEPA/TB adsorbent's active sites were loaded and blocked by Ni ions from the solution, and the mobility of Ni ions complexes in the solutions was at its greatest.

Adsorption isotherms are crucial to finding out the details about mechanisms of adsorption processes, TEPA/TB sorbent surface properties, and other parameters included in adsorption techniques. The adsorption isotherm gives a relation between the amounts of the Ni ions (mg) adsorbed on the unit mass (g) of TEPA/TB from the liquid phase and its concentration at a constant temperature. The adsorption isotherm is the elementary condition for designing any adsorption system [59].

The ideal settings for the adsorption experiments are determined by watching the most appropriate isotherm model. Different isotherms and the capacity to connect experimental results are described by the two sorption models, the Freundlich and the Langmuir models. According to the Langmuir isotherm, the following conditions must be met: the adsorption energies of the metal ions must be constant, the surface area of the adsorbent must be

uniform, and the uptake of Ni ions must take place on a uniform surface by means of a saturated monolayer of metal ions [60,61]. The following equation expresses the Langmuir isotherm model:

$$\frac{C_e}{q_e} = \frac{1}{q_{max} b} + \frac{C_e}{q_{max}} \quad (6)$$

As follows: q_e = mg/g for the equilibrium uptake of adsorbed metal ions; C_e = mg/L for the equilibrium concentration in the aqueous phase; q_{max} = mg/g for the maximum uptake of adsorbed metal ions; and b = L/mg for the Langmuir constant, which is related to the binding site affinity and the adsorption energy. Figure 6e and Table 4 show that the experimental capacity and the maximum capacity of the TEPA/TB adsorbent for Ni ions are both closer to each other, and the value of the correlation coefficient (R^2) is also closer to unity. The findings demonstrated that the processes for Ni ions removal followed the Langmuir isotherm model, which is consistent with the findings of monolayer adsorption and suggests that all of the investigated adsorbents are homogeneous in the aqueous phase.

Adsorption of Ni ions onto the surface of the TEPA/TB adsorbent is denoted by the Freundlich isotherm. Its typical application is studying the adsorbent surface's heterogeneity and energies. The adsorption process is thought to have taken place with a diverse distribution of energetic active sites, accompanied by interactions between the adsorbed metal ions [62,63]. The following equation represents the Freundlich isotherm:

$$\log q_e = \log k_f + \frac{\log C_e}{n} \quad (7)$$

This equation states that at equilibrium, the concentration of metal ions in the solution is C_e, the constant associated with surface heterogeneity is $1/n$, the total adsorption capacity of adsorbed Ni ions is k_f (mg/g), and the sorption capacity of Ni ions is q_e (mg/g), based on the information in Table 4 and Figure 6f. While the R^2 value is 0.654, the value of k_f is smaller than what is practically possible. As a result, the experimental results did not meet the Freundlich isotherm, and the adsorption mechanism did not follow the rules of heterogeneous coverage.

Table 4.
Ni ions sorption isotherm parameters of TEPA/TB

Practical uptake	Langmuir			Freundlich		
q_{ex}	q_{max}	b	R^2	k_f	n	R^2
132.50	132.81	1.293	0.999	56.56	6.04	0.654

3.2.5. Temperature and Thermodynamic

All other optimal parameters being held constant, the TEPA/TB adsorbent satisfies the temperature effect on the sorption efficiency of Ni ions within the 25-55 °C range. For the TEPA/TB adsorbent, the removal efficiency of Ni ions drops from 88.3% to 87.3% when the temperature is increased from 25 to 55 °C, as shown in Figure 7a. These findings point to an exothermic reaction, meaning that energy plays no role in the process. Since Ni ions are best adsorbed onto TEPA/TB adsorbent at room temperature, this is the best applicable temperature.

Since energy cannot be added or subtracted in an isolated system, the change in entropy is believed to be the only driving factor according to thermodynamics. When trying to predict which processes will happen naturally, environmental engineers need to think about entropy and energy. The following equations can be used to compute the thermodynamic parameters associated with the adsorption of Ni ions on TEPA/TB, namely the changes in Gibbs free energy ($\Delta G°$), enthalpy ($\Delta H°$), and entropy ($\Delta S°$) [50,64-67]:

$$K_d = \frac{q_e}{c_e} \quad (8)$$

$$K_0 = K_d \times 1000 \quad (9)$$

Here, K_d stands for the distribution coefficient. K_d is measured in liters per gram, the same as C_e, which is measured in milligrams per liter, and q_e is measured in milligrams per gram. Hence, using K_d as the equilibrium constant to compute ΔG°, ΔH°, and ΔS° is non-existent. The distribution coefficient K_d must be multiplied by 1000 to get the thermodynamic equilibrium constant K_0 (as a dimensionless variable). It is possible to estimate the values of $\Delta G°$, $\Delta H°$, and $\Delta S°$ using the following equations:

$$\Delta G° = -RT \ln K_C \quad (10)$$

$$\Delta G° = \Delta H° - T\Delta S° \quad (11)$$

$$\log K_0 = \frac{\Delta S°}{R} - \frac{\Delta H°}{RT} \quad (12)$$

With R=8.314 J/mol.K and T=absolute K, it approximated the slope and intercept of the $\log K_0$ *vs.* $1/T$ plot to get the values of $\Delta H°$ and $\Delta S°$, as shown in Figure 7b.

Table 5.
Thermodynamic coefficients at TEPA/TB for Ni ions sorption

T, °C	T, K	ΔG°, kJ/mol	ΔH°, kJ/mol	ΔS°, kJ/(mol.K)
25	298	-22.02	-2.65	0.065
30	303	-22.34		
35	308	-22.67		
40	313	-22.99		
45	318	-23.32		
50	323	-23.64		
55	328	-23.97		

As shown in Table 5, the Ni ions sorption is spontaneous, as the findings show negative $\Delta G°$ quantities at different temperatures. The negative $\Delta H°$ value specifies that the Ni ions sorption onto the TEPA/TB sorbent is exothermic in nature. Furthermore, at higher temperatures, the presence of Ni ions causes an increase in randomness at the solid-solution interface and a TEPA/TB affinity according to the positive value of $\Delta S°$. Random sorption is demonstrated to be feasible and plausible at the adsorbent/solution contact at 25 °C.

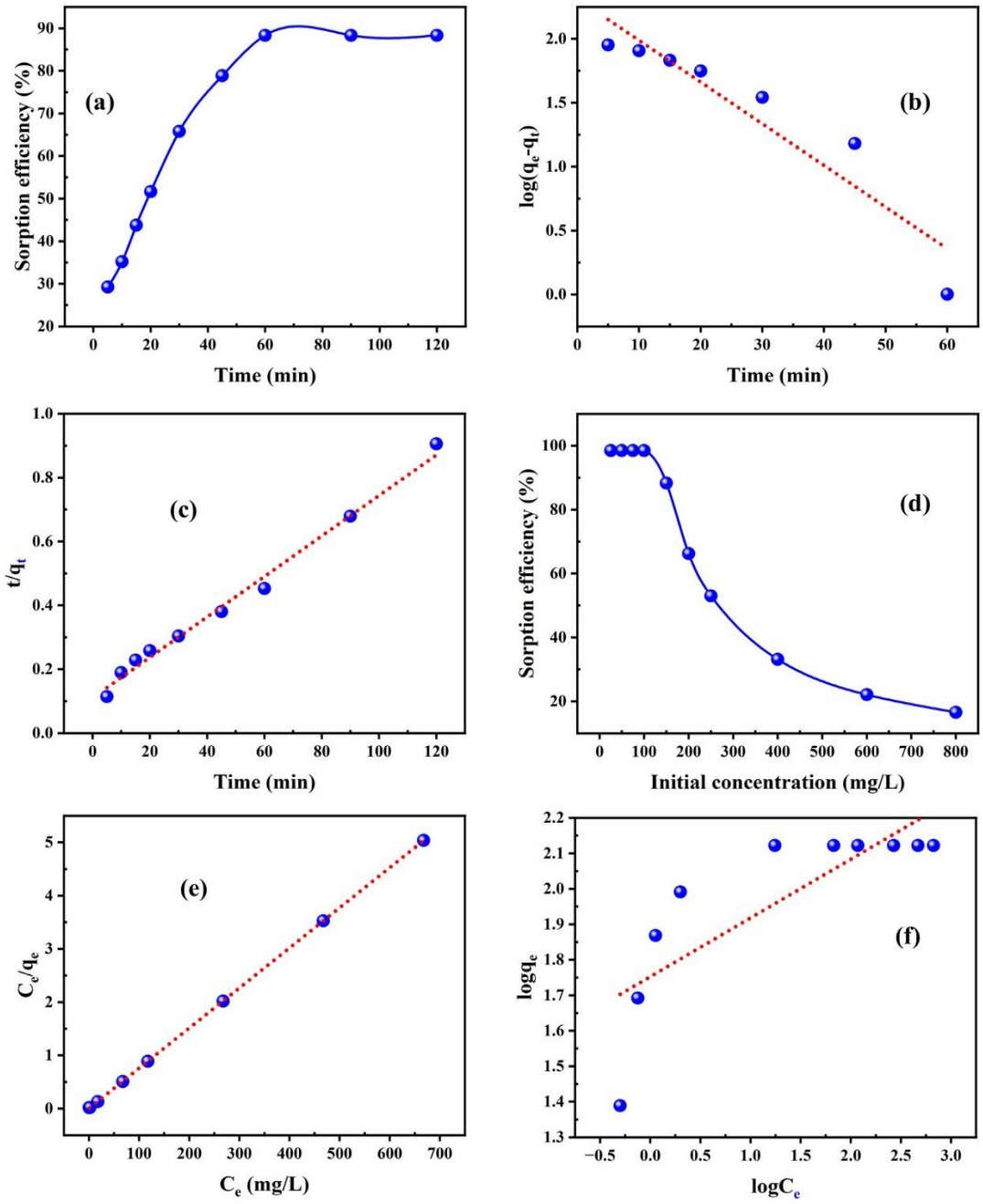

Figure 6. (a) Contact time impact on Ni ions sorption by TEPA/TB (pH 5, 50 mL of 150 mg/L Ni ions, 50 mg TEPA/TB dose, 25 °C), **(b)** PFO, **(c)** PSO, **(d)** Initial Ni ions concentration on removal efficiency (pH 5, 50 mL, 50 mg TEPA/TB dose, 25 °C, 60 min time contact), **(e)** Langmuir and **(f)** Freundlich isotherms models of Ni ions sorption

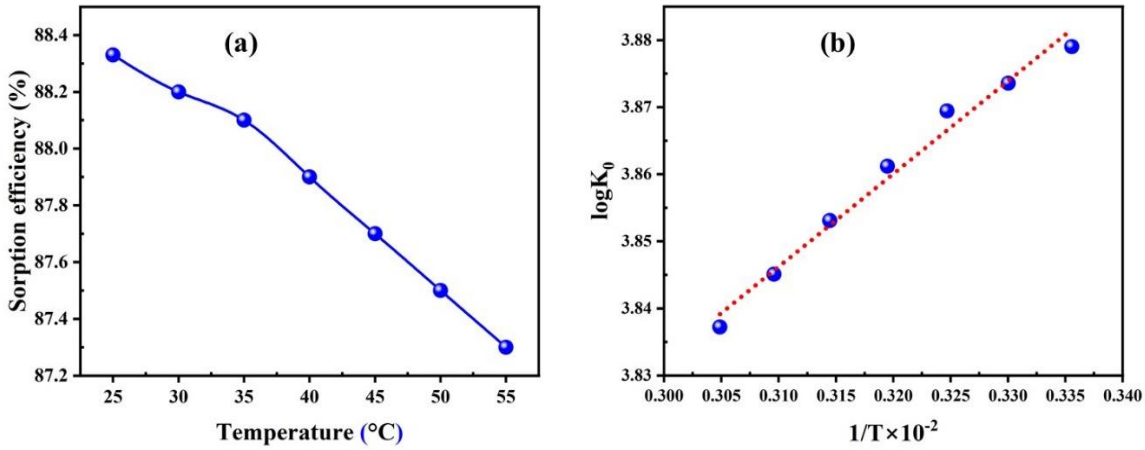

Figure 7. (a) Temperature impact, **(b)** log K_0 *vs.* 1/*T* for Ni ions sorption on TEPA/TB

3.4. Ni ions Desorption

Studying the desorption of Ni ions that were placed onto the TEPA/TB adsorbent. The desorption study is indeed used for adsorbent regeneration, and it is also the key component in lowering the cost of TEPA/TB adsorbent purification. Several experiments were conducted by mixing 1 gram of Ni ions ion-loaded TEPA/TB with 0.7 M of H_2SO_4 as a desorbing agent, swirling at 150 rpm at 25 °C for 40 minutes, and then testing the mixture. Following this, the solution was filtered, and the Ni ion concentrations were examined using the AAS method.

3.5. Regeneration

Improvements made to the TEPA/TB adsorbent through recycling are known as regeneration. The Ni/TEPA/TB is treated with 0.7 M sulfuric acid in a 1:50 S:L phase ratio and allowed to interface at room temperature for 40 minutes in order to renew the TEPA/TB adsorbent. After eight consecutive cycles, the TEPA/TB adsorbent proved to have outstanding adsorption constancy for Ni ions, with a desorption efficiency that dropped from 99.1% to 80.2%. This was achieved through repeated cycles of adsorption and desorption.

3.6. Leaching Investigates

3.6.1. Characteristics of Serpentine-Bearing Ultramafic Rocks

The rock sample that included serpentine was ground and crushed before being properly quartered and sieved. After that, the XRD and XRF chemical tests were performed on the finished sample [4]. An ultramafic rock sample that contains serpentine gained from the Um Seleimat area was analyzed chemically, as shown in Table 6. Its primary components were silica (40.35% SiO_2), magnesium oxide (38.22% MgO), iron oxide (9.88% Fe_2O_3), and nickel oxide (0.47%), which contains 3771 mg/kg Ni ions. Additionally, the serpentinite's greyish-green color and the presence of ultramafic rock attest to their enormous and intricate nature. The XRD analysis of the ultramafic rock containing serpentinite confirmed that antigorite is the dominant mineral, with forsterite being the least abundant mineral (Figure 8).

Table 6.
Significant chemical analysis of serpentinite-bearing ultramafic rocks

Constituents	Serpentinite bearing rock (%)	Constituents	Serpentinite bearing rock (%)
SiO_2	40.35	**Na_2O**	0.03
Fe_2O_3	9.88	**Cl^-**	0.02
Al_2O_3	1.13	**Co_3O_4**	0.03
MgO	38.22	**ZnO**	0.01
MnO	0.23	**NiO**	0.47
TiO_2	0.02	**SO_3**	0.05
CaO	0.47	**Cr_2O_3**	0.22
P_2O_5	0.16	**LOI**	8.45
K_2O	0.03	**Total**	**99.64**

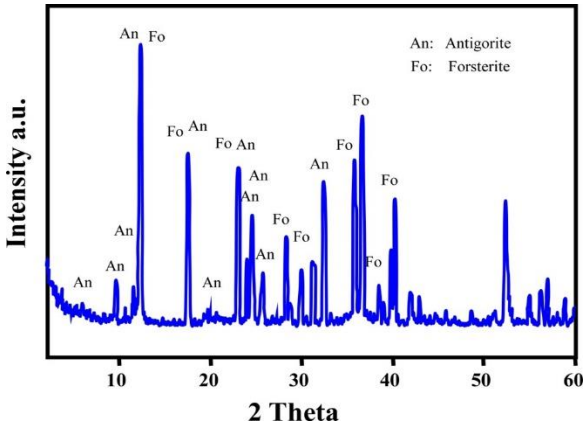

Figure 8. XRD construction of serpentinite bearing ultramafic rocks

3.6.2. Ni Ions Leaching from Serpentinite-Bearing Ultramafic Rock

Leaching is a crucial step in the processing of nickel ore because it moves the solutes from a solid to a liquid called leach. Working sample mineralogical and chemical analyses have already shown the existence of important elements like nickel. After crushing and grinding the sample to a specific size, the Ni ions leaching could be studied. We looked at leaching tests at various temperatures and with varying amounts of HCl to find the optimal conditions. The resulting slurry was filtered once the leaching experiment ended, and any remaining residue was rinsed with distilled water. The AAS was used to determine Ni ions in the filtrate that had been adjusted to a specific volume that reflected the leaching liquid. In an effort to reduce the expense of the leaching operations, various leaching parameters were examined. Among these factors were the following: leaching temperature, agitation time, solid/liquid ratio, stirring rate, grain particle size, and hydrochloric acid concentration.

3.6.2.1. Acid Type Impact

The effectiveness of Ni ions dissolution from the sample material was examined with several acid types using 2M H_2SO_4, H_3PO_4, HCl, and HNO_3. The solid/liquid ratio was 1/5, the particle size was 120 mesh, and the stirring rate was 225 rpm for 3 hours at room temperature. Ni ions leaching efficiencies are 50.6%, 46.8%, 63.5%, and 55.4% at the conditions mentioned. Figure 9a is a graphical representation of the results that were obtained. The mineral acids clearly had varying degrees of success in dissolving the Ni ions present in the material under investigation. Nevertheless, compared to the other acids, HCl achieved a greater dissolving efficiency of 63.5%. Actually, several approaches proposed for Ni ions recovery benefit from using HCl as a leachate.

3.6.2.2. HCl Concentration Impact

A number of tests were carried out to ascertain the ideal HCl concentration for Ni ions leaching from the material under investigation. Leaching was carried out at room temperature for three hours with a concentration ranging from 0.5 to 6 M, stirring at 225 rpm and using a 1/5 S/L ratio (Figure 9b). According to the results, switching from 0.5 to 4 M HCl significantly improved the Ni ions leaching efficiency, going from 41.22% to 79.41%. Increasing the acid consumption from 4 to 6 M dissolved more unwanted contaminants, particularly magnesium and iron species, leading to a severe flaw in the final product's purity.

3.6.2.3. Solid/liquid Ratio Impact

Figure 9c shows the results of an experiment that tested the effects of varying the solid-to-liquid (S/L) ratio from 1/3 to 1/10 under constant circumstances, including 4 M HCl, 225 rpm agitation rate, and a 3-hour contact time at room temperature. After the solid/liquid ratio was reduced to 1/8, the data showed that the Ni ions leaching efficiency remained consistent, increasing from 53.32% to 87.34%. Therefore, 1/8 was the ideal ratio for the following experiment.

3.6.2.4. Effect of Agitation Time

The optimal agitation duration for achieving optimum Ni ions leaching efficiency from the solid sample was determined by studying the effect of agitation time on leachability. The experiment was carried out at room temperature for a constant duration of 0.5 to 6 hours using a 4 M HCl concentration, a 1/8 solid/liquid ratio, and an agitation rate of 225 rpm. Figure 9d shows that after 4 hours of agitation, the Ni ions' leaching efficiency reached 92.35%; after this point, the solubility of Ni ions did not start to rise.

3.6.2.5. Stirring Rate Impact

Under the same conditions as before, we tested the impact of stirring rate on Ni ions leaching efficiency from 125 to 375 rpm (Figure 9e). The results on leaching efficiency showed that raising the stirring speed from 125 to 275 rpm enhanced the Ni ions's leachability from 71.56% to 94.53%. Except when the speed was over 275 rpm, it was practically constant. The remaining experiments were conducted with a stirring rate of 275 rpm.

3.6.2.6. Effect of Leaching Temperature

With a constant concentration of 4 M hydrochloric acid, a stirring speed of 275 rpm, and a solid-to-liquid phase ratio of 1/8 for 4 hours of contact time, the influence of leaching temperature was studied from 25 to 80 °C. Figure 9f shows that increasing the leaching temperature from 25 to 80 °C resulted in a slight improvement in the Ni ions leaching efficiency, going from 94.53 to 97.3%. Additionally, contaminants containing iron and magnesium ions dissolve more easily. Due to the growing number of contaminants in leach solutions and the need to save operational costs, a leaching temperature of 25 °C was selected for the actual manufacturing process.

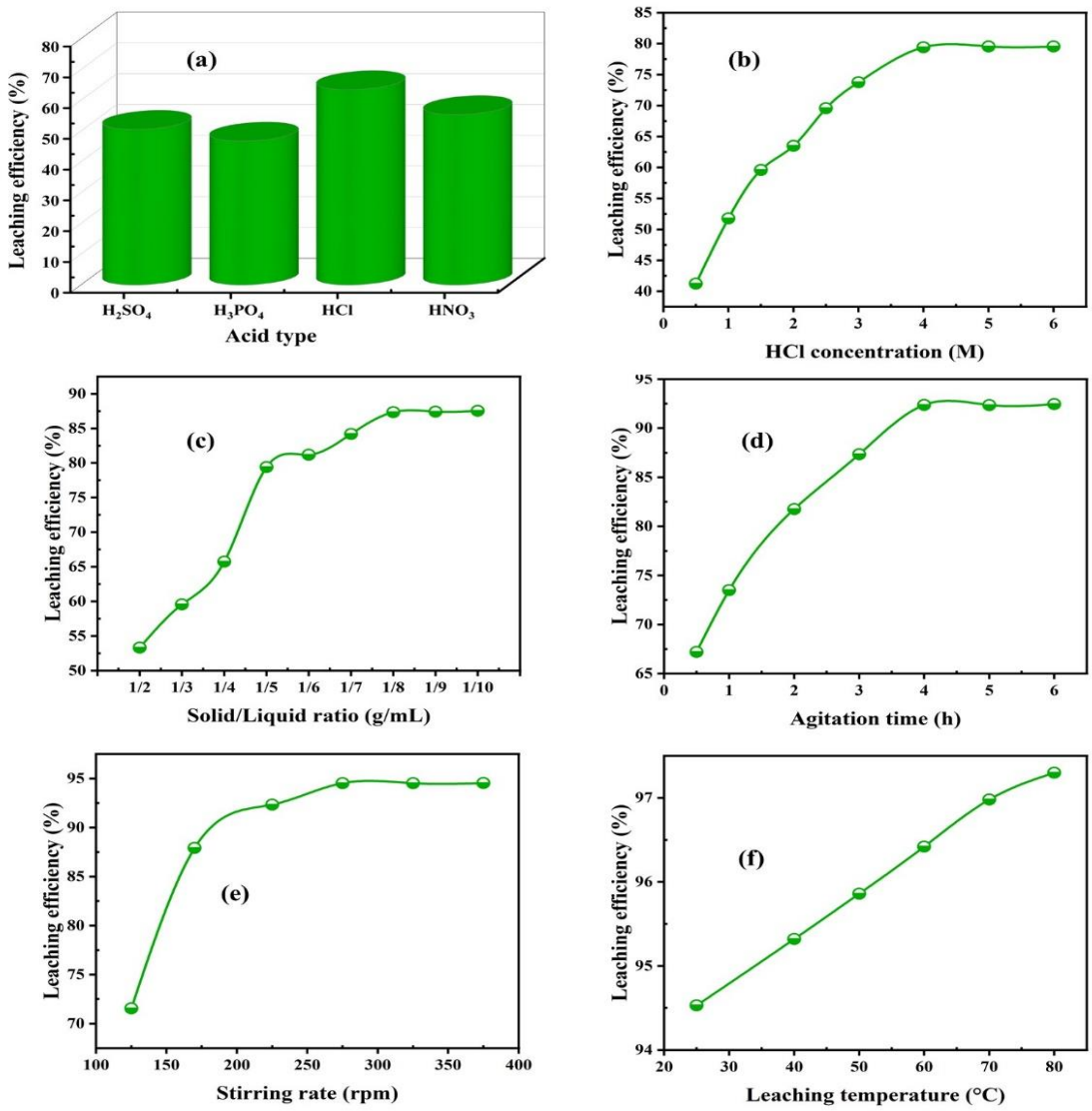

Figure 9. Effects of **(a)** leaching type, **(b)** HCl concentration, **(c)** solid/liquid ratio, **(d)** agitation time, **(e)** stirring rate, **(f)** temperature on Ni ions leaching

3.7. Ni ions Leachate Preparation

Following the ideal conditions previously established, 2 kg of the adequately ground material was mixed with 16 liters of 4 M HCl and left to agitate at room temperature for 4 hours to prepare the Ni ions leach liquid. After filtering out the insoluble gangue residue, the leaching liquid was determined to have an assay leaching efficiency of 94.53%. Table 7 shows that the leaching liquid had to adapt concentrations of Ni ions (438 mg/L Ni) and other related metals; so, it was necessary to purify the leach liquor in order to get a high-quality nickel concentrate.

Table 7.
Chemical analysis of some ions in the leach liquor using ICP-OES

Metal ions	Conc., mg/L	Metal ions	Conc., mg/L
Si^{4+}	550	Ni^{2+}	438
Fe^{3+}	2220	Cr^{3+}	15
Ti^{4+}	20	K^{+}	40
Al^{3+}	140	Ca^{2+}	77
Mg^{2+}	4430	Zn^{2+}	32
P^{5+}	110	Na^{+}	18

3.8. Ni Ions Recovery from Leachate

Impurities, including Fe^{3+}, Al^{3+}, and Zn^{2+}, were detected in the leachate chemical analysis; these ions greatly disrupt the Ni ions ion sorption and precipitation processes. Thus, in order to retrieve the Ni ions, it is necessary first to eliminate these interfering ions. Separation of Al hydroxide from the effluent liquor was achieved by adjusting the pH to 5.5 using an NH_3 solution. A pH of 3.5 would allow for the separation of the majority of iron as hydroxide.

In the end, the optimal conditions were maintained by introducing the leachate and recovering Ni ions using the TEPA/TB adsorbent. With the proper setup, 98% of the Ni ions in Ni/TEPA/TB were desorbable as $NiSO_4$. Desorption and preconcentration were performed on the solution in order to precipitate Ni ions. In order to precipitate Ni ions as nickel hydroxide, the solution was pH-adjusted to 12 with 15% NaOH [68]. For 180 minutes, the precipitate was set at 850 °C for calcination. The AAS was used to examine the newly acquired nickel oxide. Figure 10 displays the results of the EDX investigation. There was a 75.83% purity level of Ni ions in the data for nickel oxide.

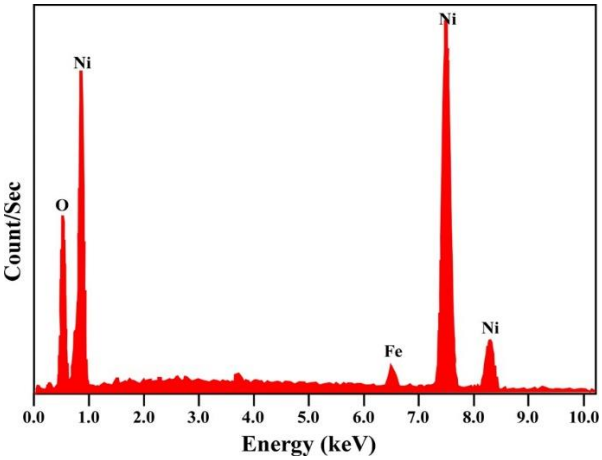

Figure 10. EDX of the gained nickel oxide

4. Conclusion

For the purpose of recovering Ni ions from the leaching liquid, a wet system produced a TEPA/TB composite by adding tetraethylene pentaamine to treated B. XRD, SEM, EDX, FTIR, BET, and Zeta potentials are used to characterize the TEPA/TB composite before and after Ni ions sorption. In batch sorption experiments, the conditions of pH 5, 50 mL of 150 mg/L Ni ions, 25 °C, and 60 minutes of contacting time were shown to have the most significant impact on the Ni ions' sorption onto TEPA/TB, indicating a value of 132.5 mg/g.

The sorption kinetics experiment further discovered that the sorption route agreed with the PSO mechanism, and the Ni ions sorption isotherm was more dependable with the Langmuir model. According to the results of the thermodynamic analysis, the sorption of Ni ions is spontaneous and possible and produces exothermic activity. Ni ions were also desorbed from Ni/TEPA/TB using 0.7 M of H_2SO_4 as a desorbing agent, swirling at 150 rpm at 25 °C for 40 minutes. The TEPA/TB sorbent was also regenerated after eight Ni ions adsorption-desorption cycles. TEPA/TB sorbent was used to recover Ni ions for leachate. Ni ions were leached from the serpentine-bearing rock using 4 M HCl, a stirring speed of 275 rpm, and a 1/8 S/L ratio for 4 hours of contact time at 25 °C. Finally, the Ni ions' adsorption-desorption on TEPA/TB was applied to gain a $NiSO_4$ solution, which was used to precipitate Ni ions as $Ni(OH)_2$. The precipitate was calcined to NiO, which has a 75.83% purity level of Ni ions.

5. CRediT authorship contribution statement

Haeam A. Abdelmonem: Conceptualization, Data curation, Validation, Investigation, Methodology, Software, Writing; **Elsayed A. Haggag:** Conceptualization, Data curation, Formal analysis, Investigation, Methodology, Writing–review & editing; **Hani E. Sharafeldin:** Leaching and separation, Investigation, Data curation, Conceptualization, Methodology, Validation, review & editing; **Khaled A. Abd El-Rahem:** Conceptualization, Methodology, Investigation, Supervision, Writing - original draft preparation, Review & Editing; **Bahig M. Atia:** Validation, Formal analysis, Investigation, Methodology, Software, Writing; **Maram M. Mohammed:** Conceptualization, Resources, Validation, Writing - Review & Editing; **Mohamed S. Atrees:** Validation, Investigation, Methodology, Software, Writing and Supervision; **Mohamed F. Cheira:** Conceptualization, Data curation, Investigation, Formal analysis, Investigation, Methodology, Software, Resources, and Supervision; **Adel E.-A. Goda:** Data curation, Formal analysis, Investigation, Methodology, Software, Validation, Visualization, Writing – original draft, Project administration, Supervision.

6. Declaration of Competing Interest

The authors declare that they have no known competing financial interests or personal relationships that could have appeared to influence the work reported in this paper.

7. References

1. Zhao, K.; Gao, F.; Yang, Q. Comprehensive Review on Metallurgical Upgradation Processes of Nickel Sulfide Ores. *Journal of Sustainable Metallurgy* **2022**, *8*, 37-50, doi:10.1007/s40831-022-00501-3.
2. Faris, N.; Pownceby, M.I.; Bruckard, W.J.; Chen, M. The Direct Leaching of Nickel Sulfide Flotation Concentrates – A Historic and State-of-the-Art Review Part I: Piloted Processes and Commercial Operations. *Mineral Processing and Extractive Metallurgy Review* **2023**, *44*, 407-435, doi:10.1080/08827508.2022.2070617.
3. Siebecker, M.G.; Chaney, R.L.; Sparks, D.L. Natural speciation of nickel at the micrometer scale in serpentine (ultramafic) topsoils using microfocused X-ray fluorescence, diffraction, and absorption. *Geochemical Transactions* **2018**, *19*, 14, doi:10.1186/s12932-018-0059-2.
4. Hamdy, M.M.; Gamal El Dien, H.; Abd El-Wahed, M.A.; Morishita, T. Garnierite-bearing serpentinite from the Central Eastern Desert of Egypt: A signature of paleo-weathering in the Arabian Nubian Shield? *Journal of African Earth Sciences* **2018**, *146*, 95-117, doi:https://doi.org/10.1016/j.jafrearsci.2017.10.007.
5. Mel, S. C. In *Encyclopedia and Handbook of Materials, Parts, and Finishes*; CRC Press: 2016.
6. Turner-Walker, G. *A Practical Guide to the Care and Conservation of Metals*; 2008.
7. Cui, F.; Wang, G.; Yu, D.; Gan, X.; Tian, Q.; Guo, X. Towards “zero waste” extraction of nickel from scrap nickel-based superalloy using magnesium. *Journal of Cleaner Production* **2020**, *262*, 121275, doi:https://doi.org/10.1016/j.jclepro.2020.121275.
8. Faris, N.; Pownceby, M.I.; Bruckard, W.J.; Chen, M. The Direct Leaching of Nickel Sulfide Flotation Concentrates - A Historic and State-of-the-Art Review Part II: Laboratory Investigations into Pressure Leaching. *Mineral Processing and Extractive Metallurgy Review* **2023**, *44*, 451-473, doi:10.1080/08827508.2022.2084735.
9. König, U. Nickel Laterites—Mineralogical Monitoring for Grade Definition and Process Optimization. *Minerals* **2021**, *11*, 1178, doi:10.3390/min11111178.
10. McDonald, R.G.; Whittington, B.I. Atmospheric acid leaching of nickel laterites review. Part II. Chloride and bio-technologies. *Hydrometallurgy* **2008**, *91*, 56-69, doi:https://doi.org/10.1016/j.hydromet.2007.11.010.
11. Quast, K.; Connor, J.N.; Skinner, W.; Robinson, D.J.; Li, J.; Addai-Mensah, J. Preconcentration strategies in the processing of nickel laterite ores part 2: Laboratory

experiments. *Minerals Engineering* **2015**, *79*, 269-278, doi:https://doi.org/10.1016/j.mineng.2015.03.016.
12. Guo, Q.; Qu, J.; Han, B.; Zhang, P.; Song, Y.; Qi, T. Innovative technology for processing saprolitic laterite ores by hydrochloric acid atmospheric pressure leaching. *Minerals Engineering* **2015**, *71*, 1-6, doi:https://doi.org/10.1016/j.mineng.2014.08.010.
13. Yunita, F.E.; Mubarok, M.Z. Nickel leaching from laterite ores by combination of organic and sulfuric acid. *AIP Conference Proceedings* **2021**, *2382*, 050003, doi:10.1063/5.0060750.
14. Sahu, S.; Kavuri, N.; Kundu, M. Dissolution kinetics of nickel laterite ore using different secondary metabolic acids. *Brazilian Journal of Chemical Engineering* **2011**, *28*, 251-258.
15. Hidayat, S.; Yulianti, S.; Anggreini, D.; Bahtiar, S. Study of Nickel Leaching Using Sulfuric Acid and Phosphoric Acid on The Selectivity Nickel Ore. *Jurnal Pijar Mipa* **2021**, *16*, 393-396, doi:10.29303/jpm.v16i3.2602.
16. Wang, R.; Ng, D.H.L.; Liu, S. Recovery of nickel ions from wastewater by precipitation approach using silica xerogel. *Journal of Hazardous Materials* **2019**, *380*, 120826, doi:https://doi.org/10.1016/j.jhazmat.2019.120826.
17. Wen, J.; Lee, M.S. Recovery of pure nickel powder from petroleum refinery sludge via a process consisting of leaching, cementation, precipitation, solvent extraction, and chemical reduction. *Journal of Chemical Technology & Biotechnology* **2023**, *98*, 2841-2850, doi:https://doi.org/10.1002/jctb.7490.
18. Silva, R.A.; Zhang, Y.; Hawboldt, K.; James, L.A. Study on Iron-nickel Separation Using Ion Exchange Resins with Different Functional Groups for Potential Iron Sub-production. *Mineral Processing and Extractive Metallurgy Review* **2021**, *42*, 75-89, doi:10.1080/08827508.2019.1678155.
19. Alvial-Hein, G.; Mahandra, H.; Ghahreman, A. Separation and recovery of cobalt and nickel from end of life products via solvent extraction technique: A review. *Journal of Cleaner Production* **2021**, *297*, 126592, doi:https://doi.org/10.1016/j.jclepro.2021.126592.
20. Kursunoglu, S.; Ichlas, Z.T.; Kaya, M. Solvent extraction process for the recovery of nickel and cobalt from Caldag laterite leach solution: The first bench scale study. *Hydrometallurgy* **2017**, *169*, 135-141, doi:https://doi.org/10.1016/j.hydromet.2017.01.001.
21. Rani, P.; Johar, R.; Jassal, P.S. Adsorption of nickel (II) ions from wastewater using glutaraldehyde cross-linked magnetic chitosan beads: isotherm, kinetics and thermodynamics. *Water Science and Technology* **2020**, *82*, 2193-2202, doi:10.2166/wst.2020.459.
22. Khedri, A.; Jafari, D.; Esfandyari, M. Adsorption of Nickel(II) Ions from Synthetic Wastewater Using Activated Carbon Prepared from Mespilus germanica Leaf. *Arabian Journal for Science and Engineering* **2022**, *47*, 6155-6166, doi:10.1007/s13369-021-06014-7.
23. Pahlavanzadeh, H.; Motamedi, M. Adsorption of Nickel, Ni(II), in Aqueous Solution by Modified Zeolite as a Cation-Exchange Adsorbent. *Journal of Chemical & Engineering Data* **2020**, *65*, 185-197, doi:10.1021/acs.jced.9b00868.
24. El-Sadaawy, M.; Abdelwahab, O. Adsorptive removal of nickel from aqueous solutions by activated carbons from doum seed (Hyphaenethebaica) coat. *Alexandria Engineering Journal* **2014**, *53*, 399-408, doi:https://doi.org/10.1016/j.aej.2014.03.014.
25. Pang, S.-k.; Yung, K.-c. Chelating Resin for Removal of Nickel Impurities from Gold Electroplating Solutions. *Industrial & Engineering Chemistry Research* **2013**, *52*, 2418-2424, doi:10.1021/ie302989v.
26. Al-Abbad, E.A.; Al Dwairi, R.A. Removal of nickel (II) ions from water by Jordan natural zeolite as sorbent material. *Journal of Saudi Chemical Society* **2021**, *25*, 101233, doi:https://doi.org/10.1016/j.jscs.2021.101233.
27. Ifijen, I.H.; Itua, A.B.; Maliki, M.; Ize-Iyamu, C.O.; Omorogbe, S.O.; Aigbodion, A.I.; Ikhuoria, E.U. The removal of nickel and lead ions from aqueous solutions using green synthesized silica microparticles. *Heliyon* **2020**, *6*, e04907, doi:10.1016/j.heliyon.2020.e04907.
28. Loutfi, M.; Mariouch, R.; Belfaquir, M.; Elyoubi, M.S. Removal of nickel from aqueous solutions using natural clay from northern morocco. *Materials Today:*

Proceedings **2021**, *45*, 7457-7467, doi:https://doi.org/10.1016/j.matpr.2021.02.018.

29. Yang, H.; Yuan, L.; Yuan, M.; Ning, P. Insight into the Mechanism of Cobalt-Nickel Separation Using DFT Calculations on Ethylenediamine-Modified Silica Gel. *Materials (Basel)* **2023**, *16*, doi:10.3390/ma16093445.
30. Awasthi, A.; Jadhao, P.; Kumari, K. Clay nano-adsorbent: structures, applications and mechanism for water treatment. *SN Applied Sciences* **2019**, *1*, 1076, doi:10.1007/s42452-019-0858-9.
31. Srinivasan, R. Advances in Application of Natural Clay and Its Composites in Removal of Biological, Organic, and Inorganic Contaminants from Drinking Water. *Advances in Materials Science and Engineering* **2011**, *2011*, 872531, doi:10.1155/2011/872531.
32. Dawodu, F.A.; Akpomie, K.G. Simultaneous adsorption of Ni(II) and Mn(II) ions from aqueous solution unto a Nigerian kaolinite clay. *Journal of Materials Research and Technology* **2014**, *3*, 129-141, doi:https://doi.org/10.1016/j.jmrt.2014.03.002.
33. Sandeep, B.; Suresha, S. NPP-modified bentonite for adsorption of Ni (II) from aqueous solution and electroplating wastewater. *International journal of environmental sciences* **2013**, *4*, 113-122.
34. Hariani, P.L.; Riyanti, F.; Fatma; Sutrini, S. Synthesis of $CuFe_2O_4$-Bentonite Composite for Adsorption of Ni (II) from Electroplating Wastewater. *Advanced Materials Research* **2015**, *1112*, 213-216.
35. Vereš, J.; Orolĺnová, Z.; Mockovčiaková, A.; Jakabský, Š.; Bakalár, T. Removal of Nickel by Natural and Magnetically Modified Bentonite. In Proceedings of the Water Treatment Technologies for the Removal of High-Toxicity Pollutants, Dordrecht, 2010//, 2010; pp. 289-294.
36. de Pablo, L.; Chávez, M.L.; Abatal, M. Adsorption of heavy metals in acid to alkaline environments by montmorillonite and Ca-montmorillonite. *Chemical Engineering Journal* **2011**, *171*, 1276-1286, doi:https://doi.org/10.1016/j.cej.2011.05.055.
37. Tirtom, V.N.; Dinçer, A.; Becerik, S.; Aydemir, T.; Çelik, A. Comparative adsorption of Ni(II) and Cd(II) ions on epichlorohydrin crosslinked chitosan–clay composite beads in aqueous solution. *Chemical Engineering Journal* **2012**, *197*, 379-386, doi:https://doi.org/10.1016/j.cej.2012.05.059.
38. Álvarez-Ayuso, E.; García-Sánchez, A. Removal of Heavy Metals from Waste Waters by Natural and Na-Exchanged Bentonites. *Clays and Clay Minerals* **2003**, *51*, 475-480, doi:10.1346/CCMN.2003.0510501.
39. Futalan, C.M.; Kan, C.-C.; Dalida, M.L.; Hsien, K.-J.; Pascua, C.; Wan, M.-W. Comparative and competitive adsorption of copper, lead, and nickel using chitosan immobilized on bentonite. *Carbohydrate Polymers* **2011**, *83*, 528-536, doi:https://doi.org/10.1016/j.carbpol.2010.08.013.
40. Bhattacharyya, K.G.; Gupta, S.S. Adsorption of Fe(III), Co(II) and Ni(II) on ZrO–kaolinite and ZrO–montmorillonite surfaces in aqueous medium. *Colloids and Surfaces A: Physicochemical and Engineering Aspects* **2008**, *317*, 71-79, doi:https://doi.org/10.1016/j.colsurfa.2007.09.037.
41. Ibrahem, W.; Mekky, H.; Khalil, A.; Belal, Z. Production of spinel forsterite refractories using sheared serpentinized ultramafic rocks, Um Seleimat, Egypt. *Journal of Engineering and Applied Sciences* **2019**, *14*, 3386-3400.
42. Kroner, A.; Greiling, R.; Kruger, J. On the tectonic evolution of the Wadi Hafafit area and environs, eastern desert of Egypt. *Precambrian Research* **1982**, *16*, A30, doi:https://doi.org/10.1016/0301-9268(82)90111-5.
43. Shalaby, A. The northern dome of Wadi Hafafit culmination, Eastern Desert, Egypt: Structural setting in tectonic framework of a scissor-like wrench corridor. *Journal of African Earth Sciences* **2010**, *57*, 227-241, doi:https://doi.org/10.1016/j.jafrearsci.2009.08.003.
44. El-Rahman, Y.A.; Polat, A.; Dilek, Y.; Fryer, B.; El-Sharkawy, M.; Sakran, S. Geochemistry and tectonic evolution of the Neoproterozoic Wadi Ghadir ophiolite, Eastern Desert, Egypt. *Lithos* **2009**, *113*, 158-178, doi:https://doi.org/10.1016/j.lithos.2008.12.014.
45. Akaad, M.K.; Noweir, A.M. Lithostratigraphy of the Hammamat–Um Seleimat District, Eastern Desert, Egypt. *Nature* **1969**, *223*, 284-285, doi:10.1038/223284a0.

46. Vimonses, V.; Lei, S.; Jin, B.; Chow, C.W.K.; Saint, C. Kinetic study and equilibrium isotherm analysis of Congo Red adsorption by clay materials. *Chemical Engineering Journal* **2009**, *148*, 354-364, doi:https://doi.org/10.1016/j.cej.2008.09.009 .
47. Alexandre, B.; Langevin, D.; Médéric, P.; Aubry, T.; Couderc, H.; Nguyen, Q.T.; Saiter, A.; Marais, S. Water barrier properties of polyamide 12/montmorillonite nanocomposite membranes: Structure and volume fraction effects. *Journal of Membrane Science* **2009**, *328*, 186-204, doi:https://doi.org/10.1016/j.memsci.2008.12.004.
48. Edathil, A.A.; Pal, P.; Banat, F. Alginate clay hybrid composite adsorbents for the reclamation of industrial lean methyldiethanolamine solutions. *Applied Clay Science* **2018**, *156*, 213-223, doi:https://doi.org/10.1016/j.clay.2018.02.015.
49. Bihannic, I.; Tchoubar, D.; Lyonnard, S.; Besson, G.; Thomas, F. X-Ray scattering investigation of swelling clay fabric: 1. The dry state. *Journal of Colloid and Interface Science* **2001**, *240*, 211-218, doi:https://doi.org/10.1006/jcis.2001.7690.
50. Cheira, M.F.; Rashed, M.N.; Mohamed, A.E.; Zidan, I.H.; Awadallah, M.A. The performance of Alizarin impregnated bentonite for the displacement of some heavy metals ions from the wet phosphoric acid. *Separation Science and Technology* **2020**, *55*, 3072-3088, doi:10.1080/01496395.2019.1675701.
51. Kostenko, L.S.; Tomashchuk, I.I.; Kovalchuk, T.V.; Zaporozhets, O.A. Bentonites with grafted aminogroups: Synthesis, protolytic properties and assessing Cu(II), Cd(II) and Pb(II) adsorption capacity. *Applied Clay Science* **2019**, *172*, 49-56, doi:https://doi.org/10.1016/j.clay.2019.02.009.
52. Cheira, M.F.; Rashed, M.N.; Mohamed, A.E.; Hussein, G.M.; Awadallah, M.A. Removal of some harmful metal ions from wet-process phosphoric acid using murexide-reinforced activated bentonite. *Materials Today Chemistry* **2019**, *14*, 100176, doi:https://doi.org/10.1016/j.mtchem.2019.06.002.
53. Horri, N.; Sanz-Pérez, E.S.; Arencibia, A.; Sanz, R.; Frini-Srasra, N.; Srasra, E. Amine grafting of acid-activated bentonite for carbon dioxide capture. *Applied Clay Science* **2019**, *180*, 105195, doi:https://doi.org/10.1016/j.clay.2019.105195.
54. Keshtkar, Z.; Tamjidi, S.; Vaferi, B. Intensifying nickel (II) uptake from wastewater using the synthesized γ-alumina: An experimental investigation of the effect of nano-adsorbent properties and operating conditions. *Environmental Technology & Innovation* **2021**, *22*, 101439, doi:https://doi.org/10.1016/j.eti.2021.101439.
55. Cheira, M.F. Synthesis of aminophosphonate-functionalised ZnO/polystyrene-butadiene nanocomposite and its characteristics for uranium adsorption from phosphoric acid. *International Journal of Environmental Analytical Chemistry* **2021**, *101*, 1710-1734, doi:10.1080/03067319.2019.1686493.
56. Sayed, A.S.; Abdelmottaleb, M.; Cheira, M.F.; Abdel-Aziz, G.; Gomaa, H.; Hassanein, T.F. Date seed as an efficient, eco-friendly, and cost-effective bio-adsorbent for removal of thorium ions from acidic solutions. *Aswan University Journal of Environmental Studies* **2020**, *1*, 106-124, doi:10.21608/aujes.2020.124579.
57. Zidan, I.H.; Cheira, M.F.; Bakry, A.R.; Atia, B.M. Potentiality of uranium recovery from G.Gattar leach liquor using Duolite ES-467 chelating resin: Kinetic, thermodynamic and isotherm features. *International Journal of Environmental Analytical Chemistry* **2022**, *102*, 2102-2124, doi:10.1080/03067319.2020.1748613.
58. Gomaa, H.; Shenashen, M.A.; Elbaz, A.; Kawada, S.; Seaf El-Nasr, T.A.; Cheira, M.F.; Eid, A.I.; El-Safty, S.A. Inorganic-organic mesoporous hybrid segregators for selective and sensitive extraction of precious elements from urban mining. *Journal of Colloid and Interface Science* **2021**, *604*, 61-79, doi:https://doi.org/10.1016/j.jcis.2021.07.002.
59. Cheira, M.F. Characteristics of uranium recovery from phosphoric acid by an aminophosphonic resin and application to wet process phosphoric acid. *2015* **2015**, *6*, 9, doi:10.5155/eurjchem.6.1.48-56.1143.
60. Allam, E.M.; Lashen, T.A.; Abou El-Enein, S.A.; Hassanin, M.A.; Sakr, A.K.; Hanfi, M.Y.; Sayyed, M.I.; Al-Otaibi, J.S.; Cheira, M.F. Cetylpyridinium Bromide/Polyvinyl

Chloride for Substantially Efficient Capture of Rare Earth Elements from Chloride Solution. *Polymers* **2022**, *14*, 954, doi:10.3390/polym14050954.

61. Allam, E.M.; Lashen, T.A.; Abou El-Enein, S.A.; Hassanin, M.A.; Sakr, A.K.; Cheira, M.F.; Almuqrin, A.; Hanfi, M.Y.; Sayyed, M.I. Rare earth group separation after extraction using sodium diethyldithiocarbamate/polyvinyl chloride from lamprophyre dykes leachate. *Materials* **2022**, *15*, 1211, doi:10.3390/ma15031211.
62. Sakr, A.K.; Abdel Aal, M.M.; Abd El-Rahem, K.A.; Allam, E.M.; Abdel Dayem, S.M.; Elshehy, E.A.; Hanfi, M.Y.; Alqahtani, M.S.; Cheira, M.F. Characteristic aspects of uranium(vi) adsorption utilizing nano-silica/chitosan from wastewater solution. *Nanomaterials* **2022**, *12*, 3866, doi:10.3390/nano12213866.
63. Hassanin, M.A.; Negm, S.H.; Youssef, M.A.; Sakr, A.K.; Mira, H.I.; Mohammaden, T.F.; Al-Otaibi, J.S.; Hanfi, M.Y.; Sayyed, M.I.; Cheira, M.F. Sustainable remedy waste to generate SiO_2 functionalized on graphene oxide for removal of U(VI) ions. *Sustainability* **2022**, *14*, 2699, doi:10.3390/su14052699.
64. Sakr, A.K.; Abdel Aal, M.M.; Abd El-Rahem, K.A.; Allam, E.M.; Abdel Dayem, S.M.; Elshehy, E.A.; Hanfi, M.Y.; Alqahtani, M.S.; Cheira, M.F. Characteristic Aspects of Uranium(VI) Adsorption Utilizing Nano-Silica/Chitosan from Wastewater Solution. *Nanomaterials* **2022**, *12*, doi:10.3390/nano12213866.
65. Tran, H.N.; You, S.-J.; Hosseini-Bandegharaei, A.; Chao, H.-P. Mistakes and inconsistencies regarding adsorption of contaminants from aqueous solutions: A critical review. *Water Research* **2017**, *120*, 88-116, doi:https://doi.org/10.1016/j.watres.2017.04.014.
66. Tran, H.N.; Nguyen, H.C.; Woo, S.H.; Nguyen, T.V.; Vigneswaran, S.; Hosseini-Bandegharaei, A.; Rinklebe, J.; Kumar Sarmah, A.; Ivanets, A.; Dotto, G.L.; et al. Removal of various contaminants from water by renewable lignocellulose-derived biosorbents: a comprehensive and critical review. *Critical Reviews in Environmental Science and Technology* **2019**, *49*, 2155-2219, doi:10.1080/10643389.2019.1607442.
67. Milonjic, S. A Consideration of the Correct Calculation of Thermodynamic Parameters of Adsorption. *Journal of the Serbian Chemical Society* **2007**, *72*, 1363-1367, doi:10.2298/JSC0712363M.
68. Mubarok, M.Z.; Lieberto, J. Precipitation of nickel hydroxide from simulated and atmospheric-leach solution of nickel laterite ore. *Procedia Earth and Planetary Science* **2013**, *6*, 457-464, doi:https://doi.org/10.1016/j.proeps.2013.01.060.